Modelling and Simulation Reveals Density-Dependent Re-Entry Risk in the Infarcted Ventricles After Stem Cell-Derived Cardiomyocyte Delivery

Leto L Riebel[1], Zhinuo J Wang[1], Hector Martinez-Navarro[1], Cristian Trovato[1], Jacopo Biasetti[2], Rafael Sachetto Oliveira[3], Rodrigo Weber dos Santos[4], Blanca Rodriguez[1]

[1]Department of Computer Science, University of Oxford, Oxford, United Kingdom
[2]AstraZeneca AB R&D, Molndal, Sweden
[3]Universidade Federal de São João del-Rei, São João del-Rei, Brazil
[4]Universidade Federal de Juiz de Fora, Juiz de Fora, Brazil

Abstract

Delivery of human pluripotent stem cell-derived cardiomyocytes (hPSC-CMs) is considered a potential therapy to improve cardiac function after injury. However, hPSC-CMs express immature electrophysiological and structural properties and may be pro-arrhythmic.

Our goal is to identify key factors determining arrhythmic risk of hPSC-CM therapy in the infarcted human ventricles through modelling and simulation. We model three densities of hPSC-CMs covering 4%, 22%, and 39% of the infarct and border zone. We furthermore simulate the effect of different therapeutic agents on re-entry susceptibility.

Due to the increased refractory period of the hPSC-CMs, the vulnerable window increases from 20ms in control, to 60ms in the low- and 80ms in the medium- and high-density scenarios.

Our results highlight the density-dependent effect of hPSC-CM delivery on arrhythmic risk after myocardial infarction and show the effect of therapeutic strategies on this increased re-entry susceptibility.

1. Introduction

Cardiovascular disease, such as myocardial infarction, is the leading cause of death worldwide. While studies have shown the ability of the human heart to regenerate [1], this happens at a slow rate, insufficient to restore cardiac function after injury. To reverse or at least halt myocardial damage, delivery of hPSC-CMs is investigated as a therapeutic option. Stem cells and stem cell-derived cardiomyocytes have been injected intramyocardially in experimental studies [2] and cultured into tissue patches later transplanted into the human heart clinically and experimentally [3, 4]. While hPSC-CMs show promising capabilities, they exhibit immature morphology and function. Properties such as slow upstroke velocity, increased action potential (AP) duration, and reduced conduction velocity might provide a pro-arrhythmic substrate when the cells are introduced into the adult human heart. Non-fatal arrhythmias have indeed been observed experimentally after delivery of hPSC-CMs [5].

Modelling and simulation can offer unique insights into arrhythmia mechanisms and the safety of different delivery configurations. In this study, we use modelling and simulation to determine the arrhythmic risk of different hPSC-CMs delivery densities in the infarcted human ventricles. Additionally, we model the effect of four therapeutic strategies and assess their ability to prevent re-entry in the pro-arrhythmic high-density scenario.

2. Methods

Electrophysiological activity is simulated using a biventricular human-based model building from single cell membrane kinetics to tissue conductivities [6]. Model parameters are altered within the infarct and hPSC-CM region. A left anterior infarct region with 75% transmurality and a border zone with a maximum width of 0.5 cm is introduced [6]. Healthy conduction velocity is set to 65, 31, and 17 cm/s in the longitudinal, transverse, and sheet normal direction, respectively as measured in [7] and reduced in the infarct and border zone by 66%.

Mesh elements are tagged as hPSC-CMs by sampling from a normal distribution taking the infarct centre as the mean, a standard deviation of 1 cm, and a cut-off radius of 2.5 cm. Low, medium, and high densities are modelled by varying the sampling size and transmurality and cover 4, 22 and 39% of the infarct and border zone (see Figure 1). Isotropic conduction velocity of 10 cm/s is set for the hPSC-CMs, in line with experimentally recorded ranges [8]. Simulations are run using a monodomain model discretised with the finite volume method [9] and linear hexahedral elements with an edge length of 0.5 mm.

The ToR-ORd [10] and Paci2020 [11] models are used to simulate the adult human ventricular, and ventricular-

like hPSC-CM AP, respectively. Electrophysiological remodelling after infarction in the infarct and border zone is modelled by scaling time constants and conductances of the fast sodium current (I_{NaF}), transient outward potassium current (I_{to}), inward rectifier potassium current (I_{K1}), rapid and slow delayed outward rectifier potassium currents (I_{Kr}, I_{Ks}), L-type calcium current (I_{CaL}) and background calcium current (I_{Cab}), as established in [6] and summarised in Table 1.

	IZ	BZ
G_{NaF}	0.40	0.38
G_{to}	0.00	
P_{Ca}	0.64	0.31
P_{Cab}	1.33	
G_{Kr}	0.70	0.30
G_{K1}	0.60	
G_{Ks}		0.20
aCaMK	1.50	
tau_{relp}	6.00	
Conduction Velocity	0.33	0.33

Table 1: Scaling factors for simulating myocardial infarction in the infarct, and border zone as in [6].

To reach steady state, three 1 Hz beats are simulated and followed by an ectopic stimulus applied on the healthy endocardial surface proximal to the border zone at 360, 380, 400, 420, 440, 460, and 480 ms after the last sinus beat. Re-entry susceptibility is measured as the window during which re-entry is inducible (vulnerable window).

Drug action of cisapride, verapamil, nitrendipine, and lidocaine is modelled as in [12] under 1 x $EFTPC_{max}$ with drug-induced current conductance changes computed using a simple-pore block model [13] (see Table 2).

3. Results

Our results, as summarised in Figure 2, show that the vulnerable window in the infarcted control (with no hPSC-CMs), and low-density scenarios, is 20 ms and 60 ms long, respectively. The vulnerable window further increases to 80 ms in both the medium, and high-density scenarios. While in the medium-density scenario the vulnerable window ranges from 380 to 460 ms after the last sinus beat, it is shifted to 400 to 480 ms in the high-density scenario.

The prolonged vulnerable window across the different densities is explained by the source-sink mismatch, and the longer refractory period of the hPSC-CMs compared to the infarcted adult tissue they replaced (see Figure 3). The hPSC-CMs present a source with elevated diastolic membrane potential and increased action potential duration. Therefore, repolarisation times in the centre of the hPSC-CM region are increased from about 355 ms in the low-density to about 435 ms in the medium density and 475 ms in the high-density scenario, close to the action potential duration at 90% repolarisation of about 480 ms in the single cell hPSC-CM Paci2020 model.

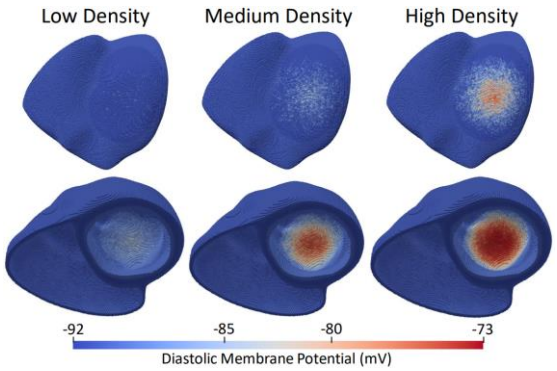

Figure 1: *In-silico* diastolic membrane potential of low (left column), medium (middle column), and high (right column) hPSC-CM densities.

Drug	G_{NaF}	G_{Kr}	G_{CaL}	G_{NaL}	G_{Ks}	G_{K1}
Cisapride		0.858				
Verapamil	0.985	0.933	0.522	0.995	0.998	0.990
Nitrendipine		0.999	0.839			
Lidocaine	0.935	0.991		0.864		

Table 2: Ionic current conductance scaling factors for four drugs under 1 x $EFTPC_{max}$ [12] using a simple-pore block model [13].

	360	380	400	420	440	460	480
Control	--	-	+	-	-	-	-
Low Density	--	+	+	+	-	-	-
Medium Density	--	+	+	+	+	-	-
High Density	--	--	+	+	+	+	-

Figure 2: Vulnerable windows for ectopic beats applied 360 to 480 ms after the last sinus beat for different hPSC-CM densities. A yellow box with a plus sign (+) marks a re-entry, while a blue box with a minus sign (-) means no re-entry is observed. A grey box with a double minus sign (--) indicates that the ectopic stimulus did not propagate.

The increased repolarisation times cause an increase in local repolarisation dispersion around the injection site, thus elevating re-entry susceptibility. This is illustrated in Figure 4, where the action potentials proximal to the ectopic stimulus location in the medium- and high-density scenarios are compared. The hPSC-CMs in the high-density scenario exhibit a more depolarised diastolic potential and longer action potential duration under sinus rhythm, resulting in the ectopic beat causing only a diminished action potential at the site of the ectopic stimulus. Hence, when the wave propagates around and then through the infarct and hPSC-CM region, the cells are stimulated again allowing for retrograde propagation and re-entry, as shown in Figure 3.

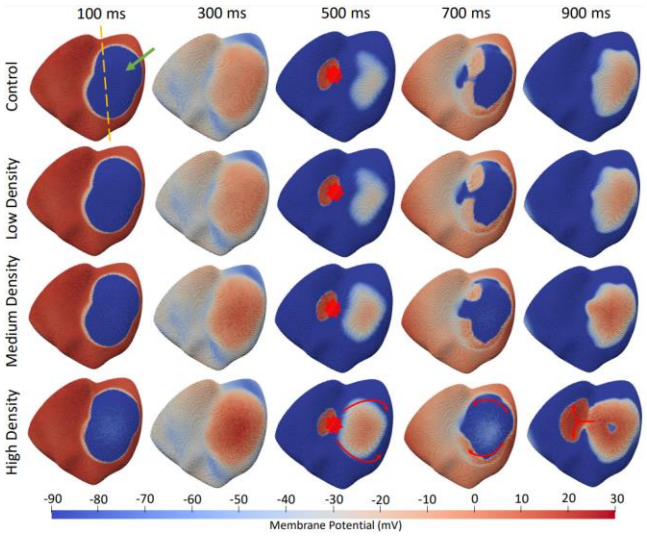

Figure 3: Electrical propagation through the infarcted human-based biventricular model in control and following the introduction of hPSC-CMs at low, medium, and high densities (with 4, 22, and 39% of infarct and border zones replaced, respectively). The green arrow in the top left points at the infarct zone in the left ventricle marking the centre of hPSC-CM delivery. The yellow dotted line represents the axis between the right and left ventricle. Re-entry is established following an ectopic stimulus applied at the endocardium proximal to the border zone at 460ms after the last sinus beat, indicated by the red star. The red arrows highlight the re-entry path.

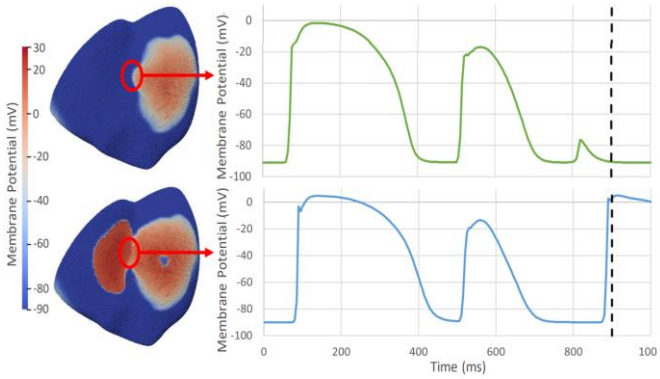

Figure 4: The images on the left show the membrane potential in the medium (top) and high (bottom) hPSC-CM density scenario at 900 ms after the last sinus beat. The red circle indicates where an ectopic stimulus is applied on the endocardial surface at 460 ms after the last sinus beat. On the right, action potentials at the ectopic stimulus site for the medium (top row, green) and high (bottom row, blue) density scenarios are shown. The first action potential is under sinus rhythm, while the second is initiated through the ectopic stimulus. Only in the high-density scenario a third action potential is triggered caused by the ectopic stimulus re-entering through the hPSC-CM area. The black dashed line indicates the time shown in the images on the left.

The increased action potential duration and refractory time of the hPSC-CM not only cause a prolongation of the vulnerable window in the high-density scenario, but also cause the ectopic stimulus applied at 380 ms after the last sinus beat to not propagate at all, as the tissue at the site of the ectopic stimulus is still refractory. Hence, while the length of the vulnerable window is maintained, its onset is delayed compared to the medium-density scenario.

In the high-density scenario, the depolarised resting membrane potential of about -73 mV as represented by the hPSC-CM single cell model is maintained. In the medium- and low-density scenario the resting membrane potential decreases to -75 and -84 mV, respectively, due to the more negative diastolic membrane potential of the surrounding adult tissue acting as an electrotonic sink. A more negative resting membrane potential decreases the spontaneous beating rate in the single cell hPSC-CM model. However, no spontaneous activity occurs in our biventricular simulations, as the spontaneous beating rate of about 0.6 Hz is suppressed by the 1 Hz sinus beat.

Figure 5 shows the effect of four different therapeutic targets, namely cisapride, lidocaine, nitrendipine, and verapamil, on the re-entry inducibility in the high-density scenario. Application of nitrendipine and lidocaine has little effect on the action potential and does not alter the vulnerable window. Cisapride, due to I_{Kr} block induced action potential prolongation, causes a delay of the vulnerable window. In contrast, application of verapamil shortens the action potential due to I_{CaL} block, which promotes the propagation of the ectopic stimulus through the infarcted tissue at earlier ectopic stimulus times.

	360	380	400	420	440	460	480
High Density	--	--	+	+	+	+	-
+ Cisapride	--	--	--	+	+	+	+
+ Lidocaine	--	--	+	+	+	+	-
+ Nitrendipine	--	--	+	+	+	+	-
+ Verapamil	--	+	+	+	+	+	-

Figure 5: Re-entry occurrence for an ectopic beat occurring 360, 380, 400, 420, 440, 460, and 480 ms after the last sinus beat for different drugs applied to the high density scenario. Blue box with minus sign (-): no reentry; yellow box with plus sign (+): reentry is induced.

4. Discussion

Here, using our 3D human-based computational modelling and simulation framework, we have shown a density-dependent arrhythmic risk of hPSC-CM delivery. We show that re-entry risk is higher after hPSC-CM delivery and increases in greater hPSC-CM densities. In our framework we consider the infarct region as electrically active as during the acute stages of infarction and propose a novel strategy to model the delivery of hPSC-CMs with respect to their density. We furthermore make use of state-of-the-art single cell models tested thoroughly against experimental data. Due to its multiscale nature, our framework allows for detailed investigation of

arrhythmia mechanisms.

Experimental studies show that improvements in left ventricular function in a guinea pig model after cardiac injury were only achieved for sufficiently high doses [14]. Therefore, while a high dose of hPSC-CMs seems necessary, it may also be arrhythmogenic, as shown in this study. Another *in silico* study [15] examined the effect of density, clustering, and location on hPSC-CM automaticity, concluding that higher cell doses promote ectopic propagation.

Our results modelling drug effects show that the vulnerable window is most sensitive to I_{Kr} and I_{CaL} block. The length of the vulnerable window is largely maintained, although the application of cisapride delays its onset. Verapamil increases the length of the vulnerable window while also bringing forward its onset. Further simulations are needed to explore more drugs and different doses. Recently, in silico simulations in tissue slabs suggested, that addressing the slow upstroke velocity and depolarised diastolic potential of hPSC-CMs may increase therapy efficiency without increasing arrhythmic risk [16]. Hence, a sodium current agonist could provide a promising solution to increase conduction velocity and, subsequently, minimise the repolarisation gradient and re-entry susceptibility.

5. Conclusion

Our simulations conclude that re-entry susceptibility in our infarcted *in silico* human-based biventricular model is density-dependent and sensitive to the block of I_{Kr} and I_{CaL}. We furthermore show that *in silico* simulations can provide a detailed tool to investigate hPSC-CM delivery parameters and contribute to identifying maximal efficacy whilst ensuring minimal arrhythmic risk.

Acknowledgments

This project was funded by a BBSRC PhD scholarship in collaboration with AstraZeneca (BB/V509395/1) to LR. BR holds a Wellcome Trust Senior Research Fellowship in Basic Biomedical Sciences (214290/Z/18/Z) and an NC3Rs Infrastructure for Impact Award (NC/P001076/1). The Paci2020 model was provided by Dr. Michelangelo Paci and the Computational Biophysics and Imaging Group (CBIG) at Tampere University Foundation. We also would like to thank UFJF, UFSJ, and Fapemig.

References

[1] O. Bergmann et al., "Evidence for Cardiomyocyte Renewal in Humans", *Science*, vol. 324, no. 5923, pp. 98-102, Apr. 2009.

[2] K.A. Gerbin et al., "Enhanced Electrical Integration of Engineered Human Myocardium via Intramyocardial versus Epicardial Delivery in Infarcted Rat Hearts", *PLoS ONE*, 10(7):e0131446, Jul. 2015.

[3] P. Menasché et al., "Transplantation of Human Embryonic Stem Cell–Derived Cardiovascular Progenitors for Severe Ischemic Left Ventricular Dysfunction", *J. Am. Coll. Cardiol*, vol. 71, no. 4, pp. 429-438, Jan. 2018.

[4] J. Yokoyama et al., "Human induced pluripotent stem cell-derived three-dimensional cardiomyocyte tissues ameliorate the rat ischemic myocardium by remodeling the extracellular matrix and cardiac protein phenotype", *PLoS ONE*, 16(3):e0245571, Mar. 2021.

[5] J.J.H. Chong et al., "Human embryonicstem-cell-derived cardiomyocytes regenerate non-human primate hearts", *Nature*, 510:273-277, Apr. 2014.

[6] X. Zhou, Z. J. Wang et al., "Ionic remodelling following myocardial infarction explains phenotypic variability in ECG and arrhythmic substrate but not in ejection fraction", *bioRxiv*, doi: 10.1101/2022.02.15.480392, 2022.

[7] B. J. Caldwell et al., "Three distinct directions of intramural activation reveal nonuniform side-to-side electrical coupling of ventricular myocytes", *Circ Arrhythm Electrophysiol.*, 2(4):433-440, Aug. 2009.

[8] J. Hansen et al., "Development of a Contractile Cardiac Fiber From Pluripotent Stem Cell Derived Cardiomyocytes", *Front Cardiovasc Med.*, 5:52, Jun. 2018

[9] R. Sachetto Oliveira et al., "Performance evaluation of GPU parallelization, space-time adaptive algorithms, and their combination for simulating cardiac electrophysiology", *Int J Numer Methods Biomed Engng.*, 34:e2913, Feb. 2018.

[10] J. Tomek et al., "Development, calibration, and validation of a novel human ventricular myocyte model in health, disease, and drug block", *eLife 2019*, 8:e48890, Dec. 2019.

[11] M. Paci et al., "All-optical electrophysiology refines populations of in silico human iPSC-CMs for drug evaluation", *Biophys J.*, vol. 118, no. 10, pp. 2596-2611, May 2020.

[12] E. Passini et al., "Human In Silico Drug Trials Demonstrate Higher Accuracy than Animal Models in Predicting Clinical Pro-Arrhythmic Cardiotoxicity", *Front Physiol.*, vol. 8, Sept. 2017.

[13] T. Brennan et al., "Multiscale modelling of drug-induced effects on cardiac electrophysiological activity", *Pharm Sci.*, vol. 36, no. 1, pp. 62-77, Jan. 2009.

[14] E. Querdel et al., "Human Engineered Heart Tissue Patches Remuscularize the Injured Heart in a Dose-Dependent Manner", *Circulation*, 143(20):1991-2006, Mar. 2021.

[15] J.K. Yu et al., "A comprehensive, multiscale framework for evaluation of arrhythmias arising from cell therapy in the whole post-myocardial infarcted heart", *Sci Rep 9*, Jun. 2019.

[16] D. Fassina et al., "Modelling the interaction between stem cells derived cardiomyocytes patches and host myocardium to aid non-arrhythmic engineered heart tissue design", *PLoS Comput. Biol.*, 18(4):e1010030, Apr. 2022.

Address for correspondence:

Leto L Riebel
Department of Computer Science, Wolfson Building, Parks Road, Oxford, OX1 3QD (UK)
leto.riebel@gtc.ox.ac.uk